A NUMERICAL STUDY OF THE IMPACT OF GREENHOUSE GASES ON THE SOUTH ATLANTIC OCEAN CLIMATOLOGY

ILANA WAINER [1], ANDREA TASCHETTO [1], BETTE OTTO-BLIESNER [2] and ESTHER BRADY [2]

[1] *Department of Physical Oceanography, University of São Paulo, São Paulo, Brazil*
E-mail: wainer@usp.br
[2] *National Center for Atmospheric Research, Boulder, Colorado, U.S.A.*

Abstract. The National Center for Atmospheric Research Community Climate System Model (NCAR CCSM, version 3) numerical coupled model is used to understand the climatic impacts on the South Atlantic Ocean due to industrialization and consequent increase of greenhouse gas emission. Two experiments are analyzed: the first one with trace/greenhouse gases at pre-industrial levels and a second one where present day levels were adopted. The results show that the annual averaged sea surface temperature, sea level pressure and barotropic transport intensify and precipitation weakens from one period to the next. With respect to the seasonal cycle, the sea surface temperature warms relative to the pre-industrial period mainly during the winter and spring; while sea level pressure presents higher values in summer and autumn. Barotropic transport has revealed significant differences between the two experiments at middle and high latitudes. Increased transport is associated with the intensification of the Subtropical Gyre and the Antarctic Circumpolar Current. Changes in barotropic transport and sea surface temperature leads to an intensification of the Polar Front and associated gradients. Examination of the precipitation field differences showed an increase over the Amazon region and along the South Atlantic Convergence Zone, during summer. The changes in sea surface temperature, sea-level pressure and barotropic transport from the pre-industrial period to the present day were more pronounced at high latitudes. These reach almost 1 °C and 11Sv between 45–60° S, respectively. Major differences in precipitation are confined to the tropics.

1. Introduction

Many studies have already shown that climate has been changing as a consequence of human activities since the Industrial Revolution due to enormous emission of greenhouse gases in the atmosphere (e.g., Hansen et al., 1998; Schimel et al., 1996; Houghton et al., 1992; Mitchell, 1989). Climate change is a global problem that, if unaddressed, could undermine progress on every aspect of human development and ecosystem protection, including food production, biodiversity, human health, and the natural systems that support growing economies (IPCC, 2001).

Carbon dioxide (CO_2) has been shown to be one of the leading greenhouse gases. Other important greenhouse gases are methane (CH_4), clorofluorcarbons (CFC11) and (CFC12), nitrous oxide (N_2O) and ozone (O_3). CO_2 emissions have increased dramatically since the beginning of the industrial age due largely to the burning of fossil fuels and deforestation. Atmospheric concentrations of CO_2 have

Climatic Change **66:** 163–189, 2004.

increased by over 30%, ranging from 280 ppmv in year 1750 to 368 ppmv in 2000 (IPCC, 2001). Petit et al. (1999) show that present day levels of CO_2 and CH_4 (368 ppmv and 1750 ppbv in year 2000, respectively) are unprecedented during the past 420 kyr.

Since the middle of the 19th century, several analyses of annual averaged surface temperature variations have shown a growth during the last century, adding up to approximately 0.6 °C (Cane et al., 1997; Houghton, 1995; IPCC, 2001). In the oceans, Levitus et al. (2000) have quantified an increase in the global temperature from the 1950s to the 1990s of 0.06 °C, which they claim, corresponds to an increase in heat content of 0.3 Wm^{-2}, between the surface and 3000 m depth. the authors believe that this observed increase in ocean heat content may be due to the increase of anthropogenic gases in Earth's atmosphere.

Crowley (2000) concludes that approximately half of the variation of temperature on decadal scale through pre-anthropogenic period (before 1850) happened due to changes in the solar irradiance and volcanism. This author suggests that the natural variability has a secondary role in the 20th century heating and that most global warming of this period should explained by anthropogenic increase in greenhouse gases concentration.

Both natural and anthropogenic forcing have to be taken into account by numerical models in order to obtain realistic simulations and predictions as shown by Stott et al. (2001) and Delworth and Knutson (2000). Future projections simulated by many numerical models (e.g., Houghton, 1995; IPCC, 2001) portray a warming of the planetary surface. Some studies have shown other consequences due to the increase in the CO_2 concentration beyond the surface warming, such as the weakening of the global thermohaline circulation (Manabe and Stouffer, 1994); the reorganization of the marine carbon cycle (Matear and Hirst, 1999); reduction of sea ice; increase in the mean sea level (Wigley and Raper, 1987); changes in precipitation patterns (Bradley et al., 1987); warmer and drier summers in continental regions in the middle latitudes (Manabe et al., 1981); increase in cyclone frequency in high latitude and intensification of storms at middle latitudes (McCabe et al., 2001) among others.

Most of the studies that deal with the problematic of increase in greenhouse gases and global warming are usually global in nature, hemispheric at most. Not much attention has been given to the South Atlantic region. Variations of the South Atlantic ocean circulation patterns and SST can occur over time scales ranging from subseasonal to the seasonal and interannual. It is thought that these variations are strongly influenced by interactions between the opposing flows of the Brazil Current and the Malvinas Current, which in turn are affected by the basin scale wind field and other atmospheric features. During the last few decades climatic variations have had an important economic and social impact on the region (SACC, 1996). Drought periods have produced changes in cattle population, drained the water supplies of large cities and caused shortages of hydroelectric power. A westward shift in rainfall that occurred during the '70s, has been related to a

significant expansion of farming in the south of Argentina, Uruguay and southern Brazil (Garzoli, 1999). The mechanisms behind these climatic fluctuations remain unclear.

This study aims to analyze, in the Climate System Model (CSM) of the National Center for Atmospheric Research (NCAR), the impacts of global warming on the general characteristics of the mean climatology of the South Atlantic region due mainly to industrialization and consequent increase in greenhouse gas concentrations.

2. The Numerical Model

Coupled models used in climate change studies have undergone a rapid development in recent years and have in several respects obtained a considerable degree of realism. The National Center for Atmospheric Research (NCAR)-Community Climate System Model (CCSM) consists of 4 components: atmosphere, ocean, land surface and sea-ice (the reader is referred to Boville and Gent (1998) for more details).

The atmospheric component is the Community Climate Model, version 3, with T42 resolution (approximately 2.8° in latitude and longitude) and 18 vertical layers (Kiehl et al., 1998; Hack et al., 1998). The ocean component of this model was developed from the Geophysical Fluid Dynamics Laboratory z-coordinate primitive equation model (Gent et al., 1998). The spatial resolution is 2.4° in longitude, with variable resolution in latitude ranging from 1.2° to 2.3°, and 45 vertical levels. The meridional resolution is 2.2° at 20°S and 1.8° at 40°S. The sea-ice model dynamics is based on the cavitating fluid rheology by which the ice pack does not resist divergence or shear, but does resist convergence (Flato and Hibler, 1992; Weatherly et al., 1998). The land-surface model provides a comprehensive treatment of land surface processes allowing for different vegetation types (Bonan, 1998). Although the land-surface model computes river runoff, it is not transferred to the ocean model. The interaction between river runoff and shelf processes, a significant problem of human-scale relevance, has now been implemented in a later version of the coupled model.

Two experiments are run with different levels of greenhouse gases to study the sensitivity of the South Atlantic Ocean to their changes. The pre-industrial experiment adopts the concentrations of trace gases, estimated from ice core records: 280 ppmv for CO_2, 700 ppbv for CH_4, 275 ppbv for N_2O, and no clorofluorcarbons. The appropriate solar constant is 1365 Wm^2. The present day (post-industrial) experiment differs from the previous one by the amount of greenhouse/trace gases which are specified for current atmospheric conditions (1990s) with the following gas concentrations: 354.4 ppmv for CO_2, 1722.3 ppbv for CH_4, 308.4 ppbv for N_2O, 514.0×10^{-3} ppbv for CFC11 and 462.7×10^{-3} ppbv for CFC12. The solar constant was fixed at 1367 Wm^2.

Each experiment was run for 150 years. The model data analyzed consists then of the climatology computed by using monthly mean output of sea surface temperature (SST), sea level pressure (SLP) and barotropic streamfunction (PSI). The focus is on the South Atlantic Ocean region, defined to be between the Equator and 60° S and from 80° W to 20° E.

3. Results

The model data analyzed are monthly mean output from 150 years of a control run of the CCSM. Model results are initially compared to the surface fields from the annual climatologies of Hellerman and Rosenstein (1983), the DASILVA 1945–1989 (Da Silva et al., 1994) which is based on COADS, but has improved resolution and boundary layer parameterizations and the Reynolds and Smith (1994) climatology, which was constructed using sea surface temperature fields blended from ship, buoy and bias-corrected satellite data.

The dominant feature of the South Atlantic simulated annual mean surface winds in the CCSM and in the observations is the broad subtropical anticyclone. The wind-stress in Nm^{-2} are overlaying the mean annual SSTs, °C, and can be seen in Figure 1. Figures 1c all show a weak southwest-northeast gradient north of 35° S, where the isotherms are predominantly zonal south of that. The figure shows that, although the overall broad gyre wind circulation patterns are very similar, the wind-stress derived from the model is stronger. In fact, the CSM annual-mean zonal wind-stress component (not shown) is almost twice the value of the DASILVA climatology, except approximately 3° either side of the zero line. The meridional component of the wind-stress in the CSM is also stronger, in particular between 20° W and 15° E where differences are on the order of 0.03 Nm^{-2}. The global annual-mean CSM wind-stress is also stronger compared to the NCEP reanalysis product as shown by Danabasoglu (1998).

A coarse resolution model, such as the CCSM, can successfully reproduce major features of the South Atlantic region, further details can be found in Wainer et al. (2000). Therefore, the impact of global warming with the two experiments designed to simulate pre-industrial en present day conditions can be further explored. The annual mean and seasonal climatology for the pre-industrial simulation results are discussed next, together with their difference relative to the present day simulation,

3.1. THE SEA SURFACE WARMING

The pre-industrial SST annual climatology is shown again in in Figure 2a together with the corresponding variance field (Figure 2b). The highest variance is located right at the Brazil Malvinas Confluence (BMC) region with a maximum of 22 $°C^2$, at 55° W, 40° S.The BMC is a frontal zone formed by the merging of the south-

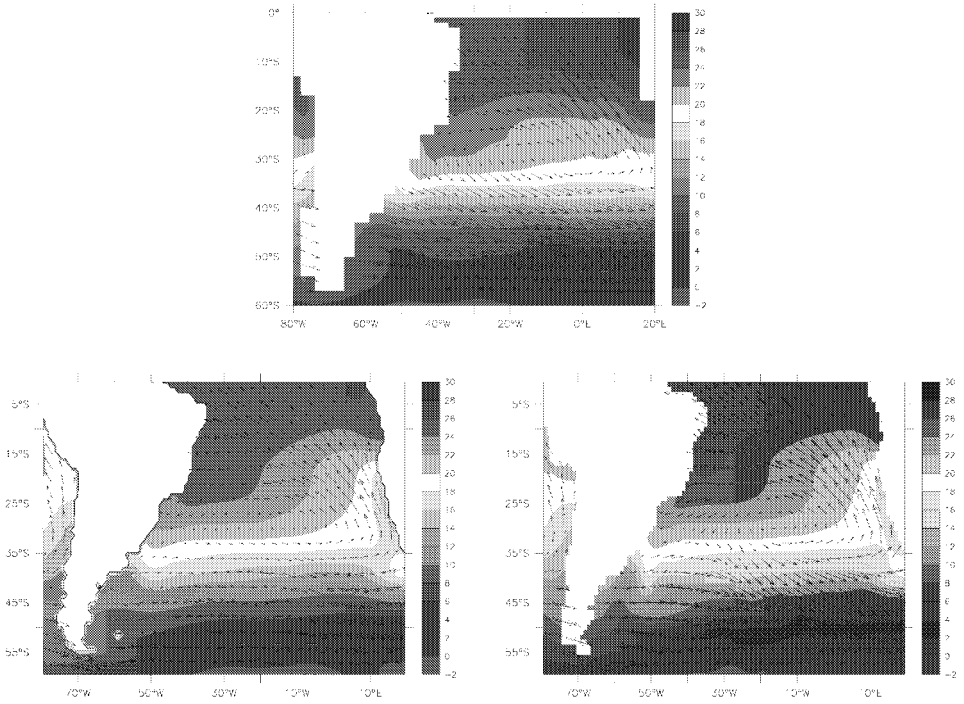

Figure 1. Annual mean SST and wind stress for (a) the post-industrial simulation, (b) DASILVA and (c) IGOSS (SST) and HR (wind stress). Contour interval is 2 °C and maximum vector is 0.16 Nm^{-2}.

ward flowing, warm and salty Brazil Current and the northward flowing, cold and relatively fresh Malvinas Current.

The corresponding seasonal climatology (Figures 2c–f) is characterized as expected, by the warming of surface waters in summer and cooling in winter. The southeastern coast of South America presents the larger SST gradients and a displacement of cold waters next to the BMC region. The cold waters reach lower latitudes on the South America coast during winter (Figure 2e).

Figure 3 shows the annual cycle for SST averaged over the whole South Atlantic Ocean for the two experiments. The solid curve represents the pre-industrial results while the dashed line shows the results for the 1990s. One notices that there is agreement in the phase of the seasonal cycle but there are significant changes in magnitude, in particular from June to October with a maximum of 0.91 °C in September.

In order to show that the magnitude of this warming is realistic, we average the first two and last two decades of the observed-based SST product from 1900–1999 of the Hadley Centre Global Sea Ice and Sea Surface Temperature (HadISST) Analyses (Rayner et al., 2003). The two curves can be seen in Figure 4. Although there is a significant warming in the South Atlantic region from the beginning of

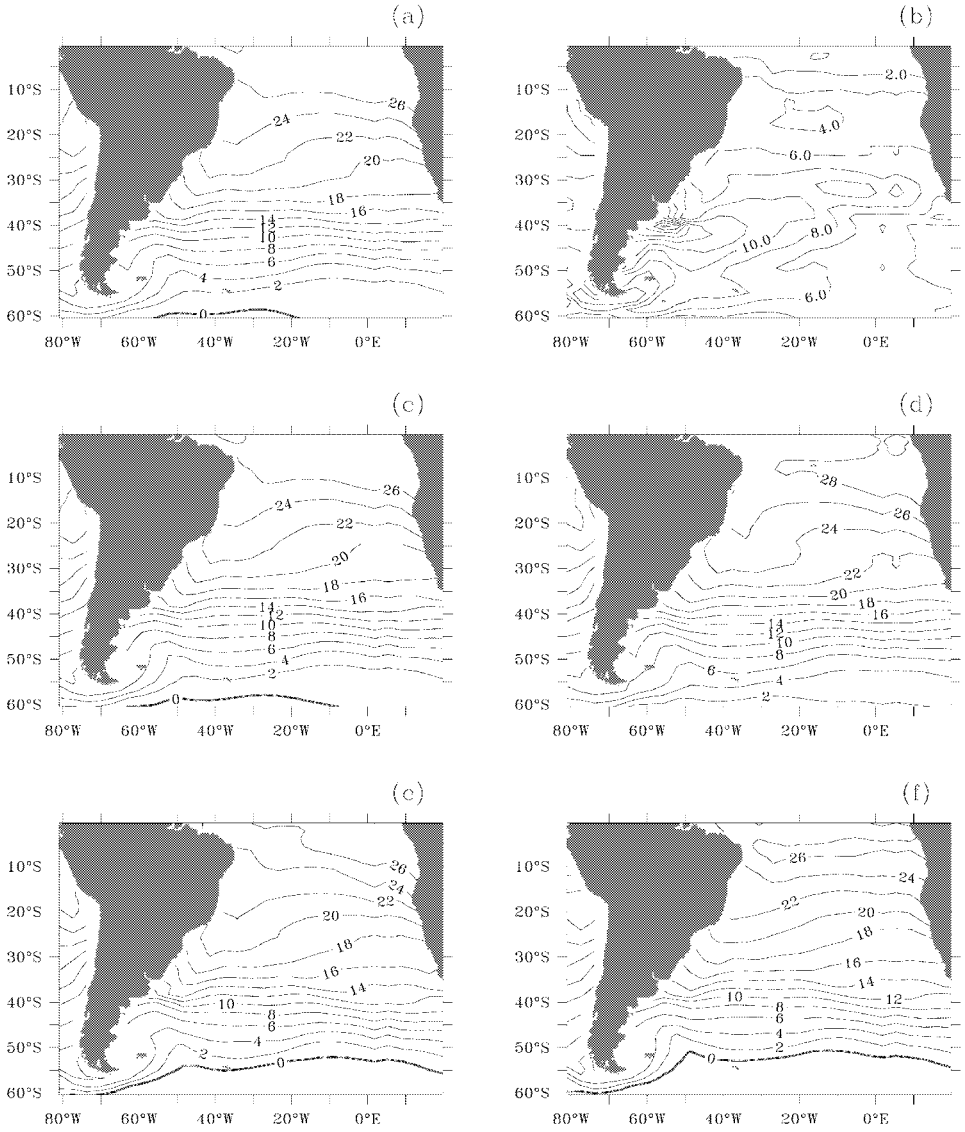

Figure 2. (a) SST annual climatology for the pre-industrial period. (b) The associated SST variance (contour interval is 2 °C^2). SST seasonal climatology for the pre-industrial period: (c) summer; (d) autumn; (e) winter and (f) spring. Contour interval is 2 °C.

the century to present day with magnitude comparable with the simulations, the warming is more uniformly distributed throughout the year.

The time versus latitude difference of the zonal mean SST can be seen in Figure 5. Positive values indicate warming indicating that there was warming in almost all of the South Atlantic basin throughout the year, except at mid-latitudes and south of 55° S from February to May where there is cooling below –0.4 °C. It can

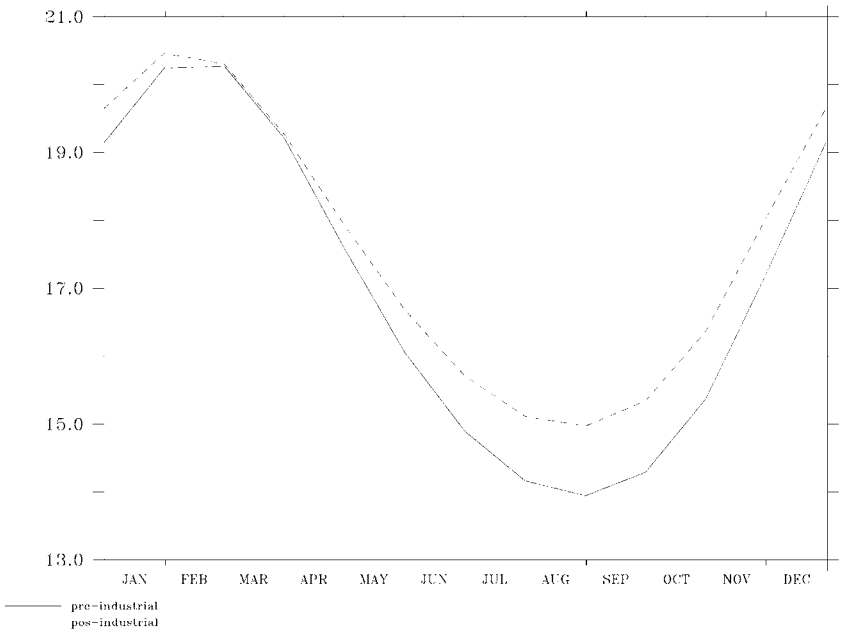

Figure 3. Annual cycle of SST averaged for the whole South Atlantic domain in °C. Black curve represents the pre-industrial simulation results while the dashed curve represents the present day results.

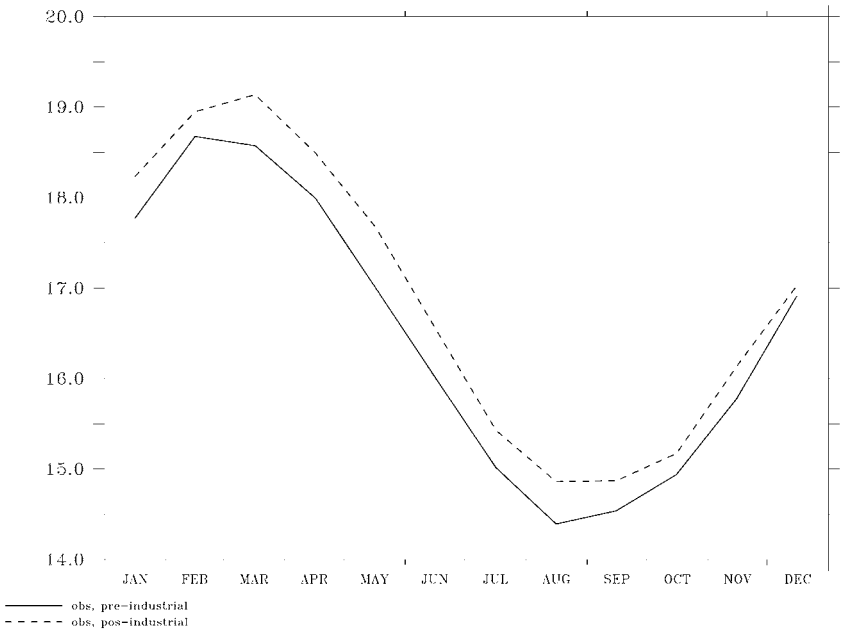

Figure 4. Annual cycle of HadiSST (Rayner et al., 2003) SST averaged for the whole South Atlantic domain in °C. Black curve represents the average for pre-industrial years (from 1900 to 1920) while the dashed curve represents the present day results (average from 1970 to 1990).

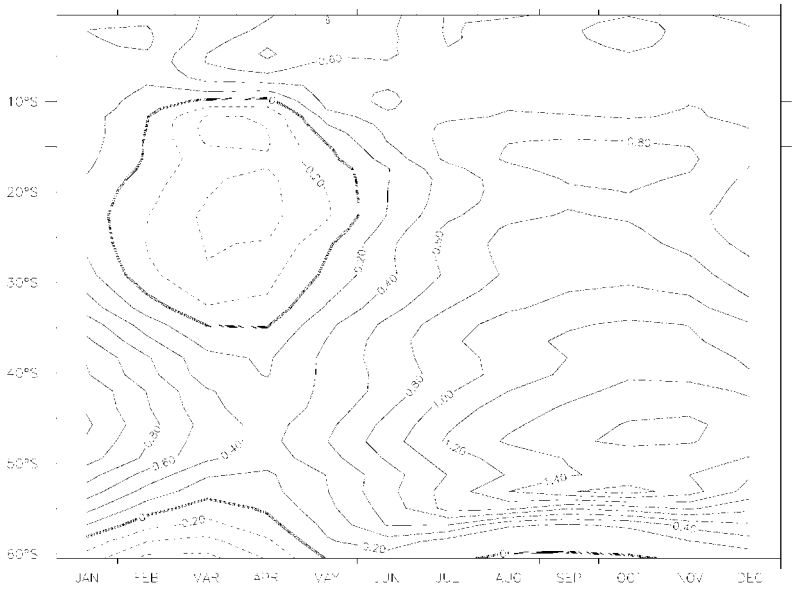

Figure 5. Difference between zonal mean SST from the two simulations (present day–pre-industrial). Contour intervals is 0.2 °C.

also be seen in Figure 5 the increase of SST between 35–55° S exceeding 1.6 °C, at 45 °S, during October and November. This suggests a warming at the northern edge of the Antarctic Circumpolar Current (ACC). According to Gille (2002) mid-depth Southern Ocean temperatures have indeed increased between the 1950s and the 1980s, mostly within the ACC.

In fact, the strong positive gradient across 58° S (Figure 5) from July to December, indicates changes in the Subantarctic and Antarctic frontal zones which leads to a strengthening of the Polar Front (which lies between 55° S to 60° S, approximately). To the south of this region, SST does not increase very much. According to Stouffer et al. (1989), the CO_2-induced warming of SST in the southern limit of the ACC is slower because of a reduction in the deep oceanic mixing of heat associated with a weakening of thermohaline circulation. Manabe and Stouffer (1994) showed via numerical simulations that such a delay disappears when CO_2 concentration is quadrupled over the period of several centuries.

The spatial structure of the SST difference between pre- and post-industrial simulations can be seen in Figure 6a. The strongest warming signal is found south of 50° S, between the longitudes of 40° W and 10° W where it reaches a maximum value of 1.4 °C around 20° W–50° S. It can also be seen that there are regions where the increase in temperature is not as evident. For example, the small area in the eastern Brazilian coast that extends to 20° W, and another one throughout 60° S latitude, in the east of 60° W.

The first semester (Figures 6b,c) presents both relative warming and cooling, consistent with Figure 5. During summer (Figure 6b), positive differences (warm-

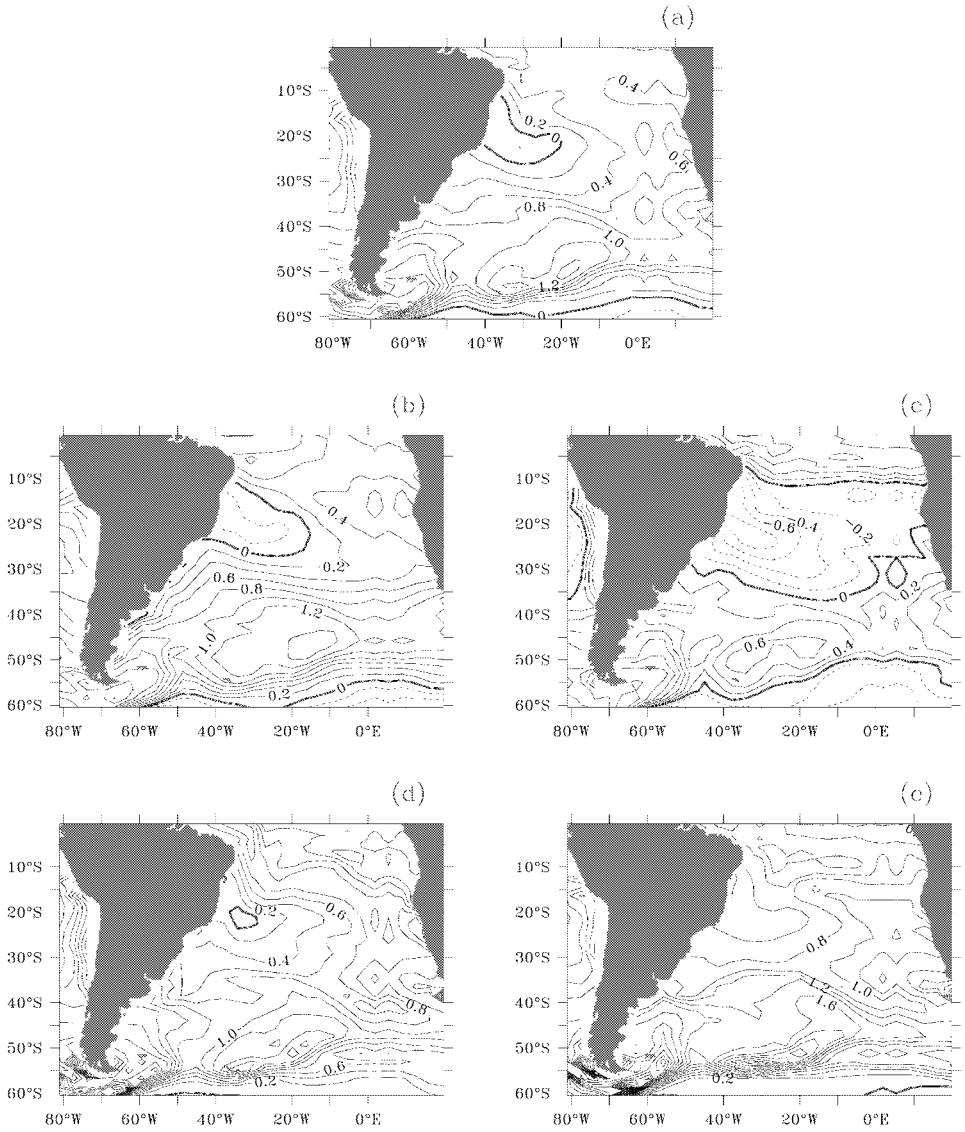

Figure 6. (a) SST difference between the two simulations (present day–pre-industrial) for the annual climatology. Contour intervals is 0.2 °C. SST difference between the two simulations (present day–pre-industrial) for the seasonal climatology: (b) summer; (c) autumn; (d) winter and (e) spring.

ing) exists throughout the basin. Negatives differences (cooling) are found both at the northeastern part and throughout the 60° S latitude band. In autumn (Figure 6c) it is possible to notice bands of relative cooling between 10° S and about 35° S and to the south of approximately 55° S. These are zonally elongated with warming regions in between (north of 10° S and between 35° S and 50° S). In the winter months (Figure 6d) the South Atlantic is dominated by positive differences

of temperature, representing an average warming from the pre-industrial period to the present. A small core of null differences exists centered at 20° S–37° W. Finally, in spring (Figure 6e), the warming is intensified, with highest differences along the ACC, exceeding values of 2.5 °C. The strong gradient of SST difference between 50° S and 60° S can be associated with the meeting of cold waters brought northward and mid-latitude originated warm waters, suggesting the intensification of the Polar Front.

3.2. CHANGES ASSOCIATED WITH THE SUBTROPICAL HIGH

The South Atlantic is characterized by a high-pressure center located in the central part of the ocean, associated with values as high as 1020 mb, representing the South Atlantic Anticyclone (Figure 7a). Southward of 40° S, the pressure field becomes more zonal and shows a more pronounced southern gradient. In this region one notices basin-wide westerlies (i.e., Figure 1). Over the continent the SLP has lower value and higher variance (approximately 20 mb^2, around 25° S, 55° W), as seen in Figure 7b.

The high-pressure center of the South Atlantic (also known as the Subtropical High) is more intense in the winter than in summer (Figures 7c,e) as opposed to the centers of high SLP over the other oceans. The Subtropical High moves seasonally, being located more towards southern latitudes in summer (Figure 7c) and towards the equator in winter (Figure 7e). This shift is accompanied by the migration of the Intertropical Convergence Zone (ITCZ) that determines to a great extent, the rainy season in the Brazilian Northeast (Hastenrath, 1991). The SLP differences at mid ocean basin and off the coasts of South America and southeast Africa are larger in summer, therefore the winds along the western coast of Africa and the associated upwelling are also stronger.

The major differences between the averaged SLP results for the two simulations occurs during austral summer (Figure 8). The differences for the zonal mean SLP (Figure 9) indicate an intensification (positive contours) of the present day spatial pattern. It can be noted that the major difference occurs from January to May exceeding values of 200 mb at 50° S, in February. In April, the northern limit of the Southern Atlantic Subtropical High is more intense by 150 mb. In the following months, the main SLP differences are found to the south of 40° S. Across 50° S, for example, the SLP is intensified in February, weakened by 50 mb in June–July and increases again by 100 mb in September. This behavior could imply in a meridional shift of the associated westerly wind region.

The spatial structure of the annual differences are best observed in Figure 10a. SLP differences between pre-industrial and present day shows predominantly positive values that are larger throughout a diagonal band that crosses the Atlantic from the Brazilian northeast coast (approximately centered at 15° S–40° W to 50° S–0° W). Over the continent the differences are almost insignificant, with a small region around 32° S–68° W, where SLP decreases.

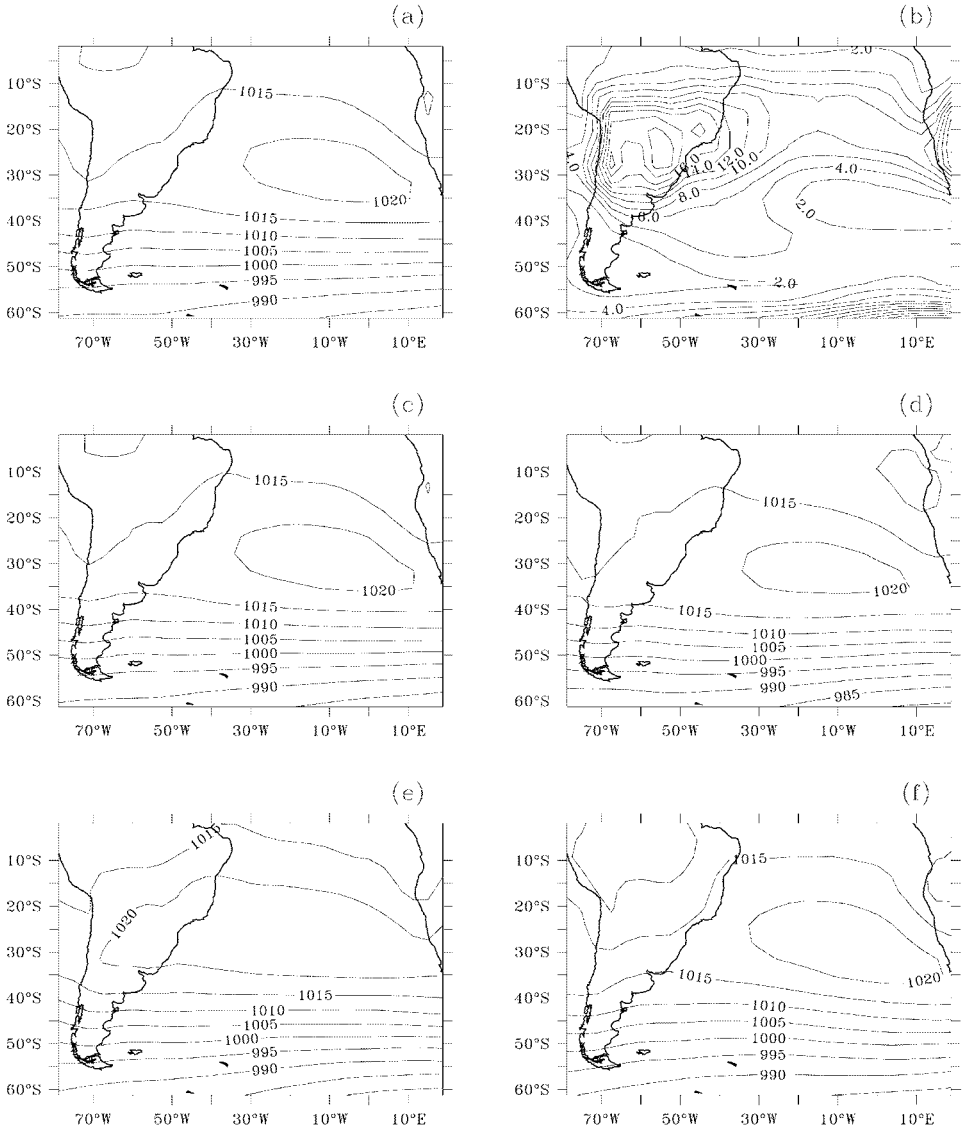

Figure 7. (a) SLP annual climatology for the pre-industrial period. (b) SLP variance (contour interval is 2 mb^2). SLP seasonal climatology for the pre-industrial period: (c) summer; (d) autumn; (e) winter and (f) spring. Contour interval is 5 mb.

In the seasonal analyses (Figures 10b–e) it is possible to notice considerable differences throughout the year, mainly during summer (Figure 10b). This difference is most evident at 30° W–45° S where it reaches almost 2.0 mb. In autumn (Figure 10c) results show SLP differences higher than 1.8 mb around 35° W–25° S. In winter (Figure 10d) the situation reverses (difference of –1.2 mb, around 55° S–30° W. The tip of South America shows an intensification of the SLP pattern.

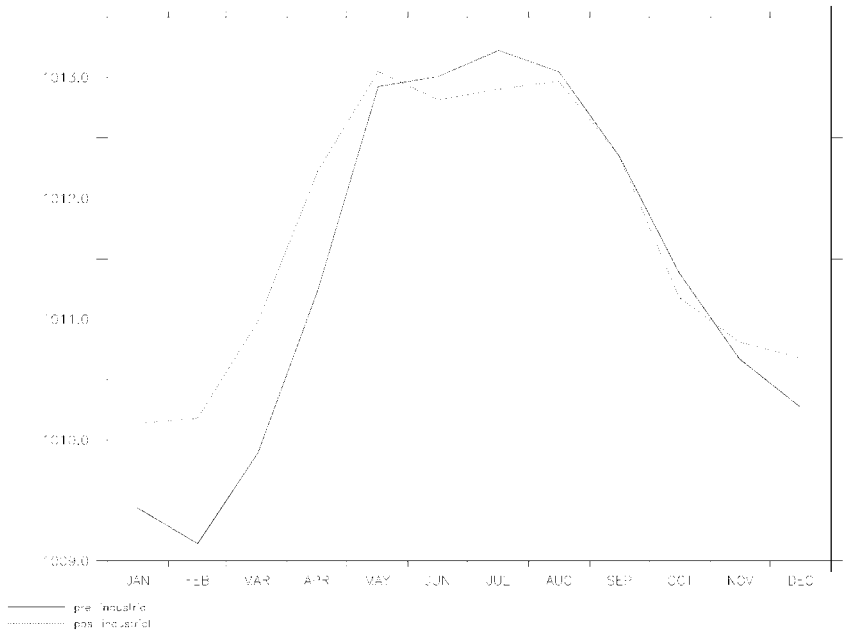

Figure 8. Annual cycle of SLP averaged for the whole South Atlantic domain in mb. Black curve represents the pre-industrial simulation results while the dashed curve represents the present day results.

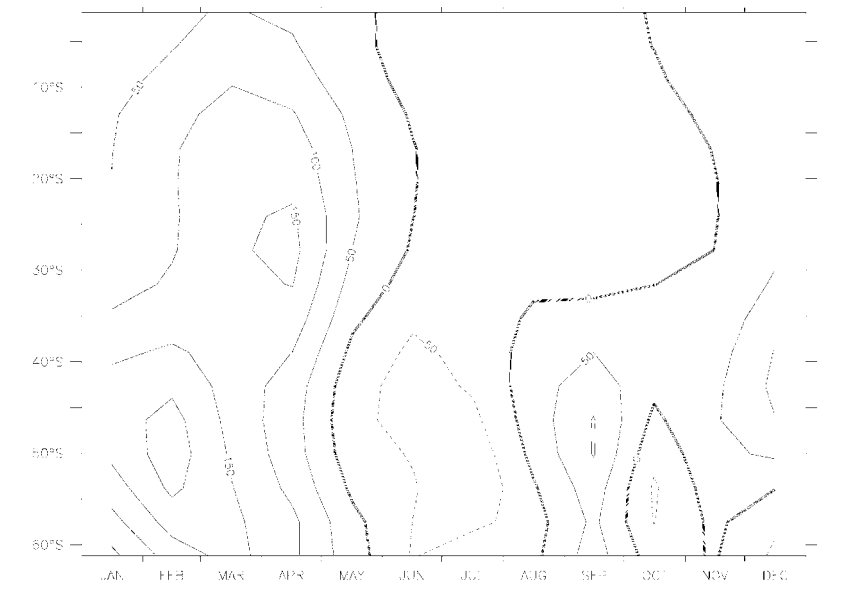

Figure 9. Difference between zonal mean SLP from the two simulations (present day–pre-industrial). Contour intervals is 50 mb.

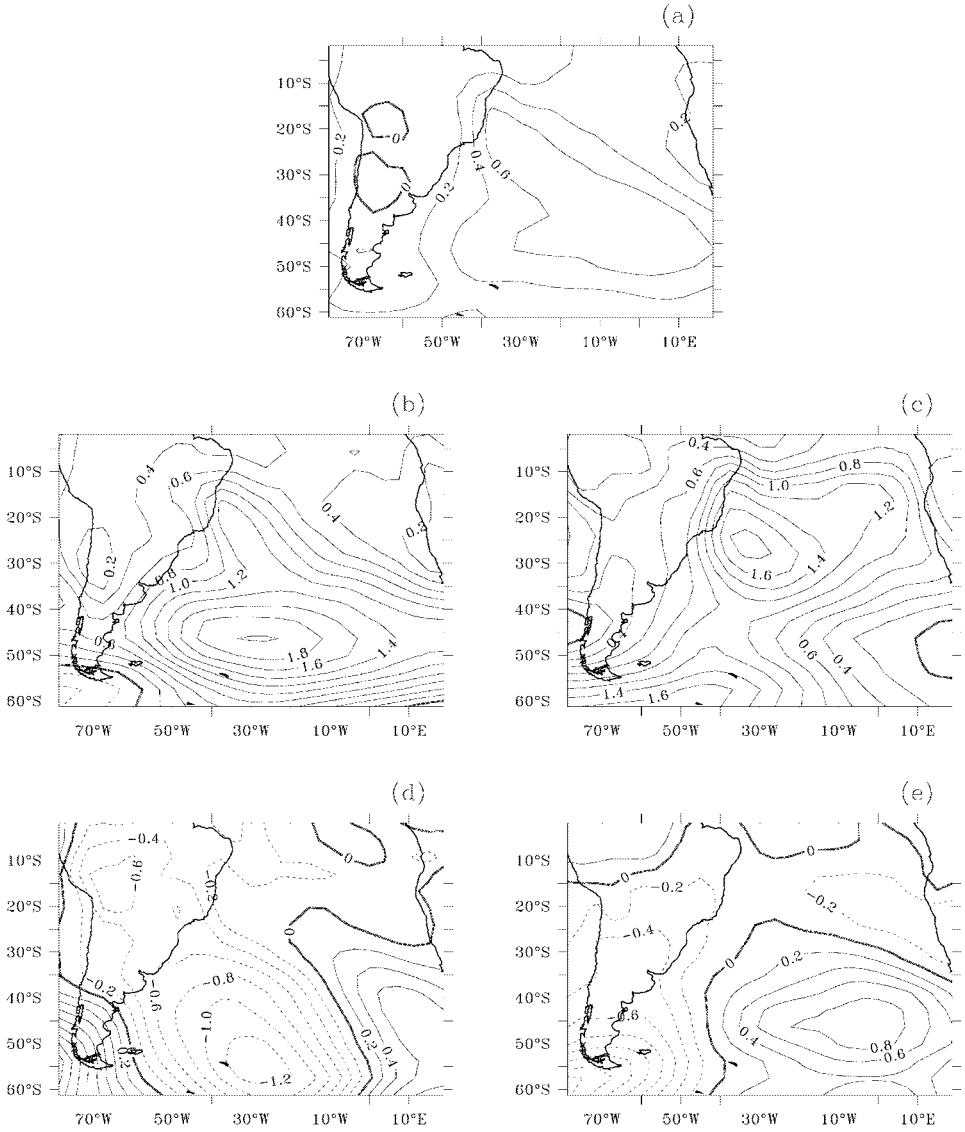

Figure 10. (a) SLP difference between the two simulations (present day–pre-industrial) for the annual climatology. Contour intervals is 0.2 mb. SLP difference between the two simulations (present day–pre-industrial) for the seasonal climatology: (b) summer; (c) autumn; (d) winter and (e) spring.

In spring (Figure 10e) the SLP changes are smaller, with positive differences of 0.8 mb throughout 45° S between the longitudes of 20° W and 5° E, and negative differences over the continent, more evident farther to the south. It should be noted that the equatorial region shows very little changes throughout the year.

3.3. THE INTENSIFICATION OF ANTARCTIC CIRCUMPOLAR CURRENT

The barotropic stream function (PSI) represents the vertically integrated advective transport over the entire water column. The PSI annual climatology is presented in Figure 11a. Negative values of PSI are observed in the central region of the South Atlantic representing the transport within the subtropical gyre. In the southern part of the Atlantic Basin, positive values of the stream function associated with northward transport are shown. The higher values of PSI are associated with the ACC, between 50° S and 60° S. To the south of 35° S approximately, PSI variance increases reaching values as high as 160 Sv at the ACC region (Figure 11b). The ACC is is the world's only current that completely encircles the globe. Unlike the other oceans of the world where the transport depends on the curl of the wind stress, ACC transports are due to the wind stress itself. Thus, this mechanism dictates that the ACC must be a deep current reaching to the lower depths of the ocean which justifies looking at the barotropic stream function.

The seasonal climatology for the pre-industrial PSI can be seen in Figures 11c–f. During winter (Figure 11e) the barotropic transport is stronger than that in summer south of 40° S (Figure 11c). North of 40° S the transport is more intense in the autumn (Figure 11d) and can be associated to the Angola Dome (Reid, 1989).

Stramma and Peterson (1989) estimated a geostrophic transport of the northern Benguela Current of 21 Sv at 32° S in the upper layer, while both experiments here analyzed, show a transport around to 15 Sv at 32° S, 10° E. Miranda and Castro (1982) estimated a transport for the Brazil Current at 19° S of 6.5 Sv with respect to a reference level of 500 m. In the annual average, the transport simulated in both experiments shows approximated values of 20 Sv at 25° S, 40° W. PSI to south of 50° S, in the two experiments, seems to be overestimated probably because of the stronger winds in the simulations.

The annual cycle of the barotropic transport averaged for the whole region (Figure 12) reveals a significant increase from one period to the next of about 2.5 Sv in March and July. Figure 13 shows the difference of zonal mean PSI between the two simulations. Between December and June the 10–30° S latitudinal band is intensified, reaching 4 Sv more in April from the present day level simulation to the pre-industrial one. In the following months it is weakened by 2 Sv in July and August. The southern part of subtropical gyre is strengthened throughout the year with more intensity from August to November when the PSI difference reaches 4 Sv. The main feature in Figure 13 is the gradient of positive differences to south of 45° S that can be associated with an intensification of the ACC (more pronounced throughout the 55–60° S band). In April, PSI is almost 20 Sv higher in post-industrial simulation than in the pre-industrial experiment.

The spatial structure of these annual differences (Figure 14) are most pronounced at the southwest edge of the domain, centered around 55° S–0° E. The seasonal differences of the barotropic transport between the two experiments are presented in Figures 14b–e. The biggest changes from pre-industrial to present day

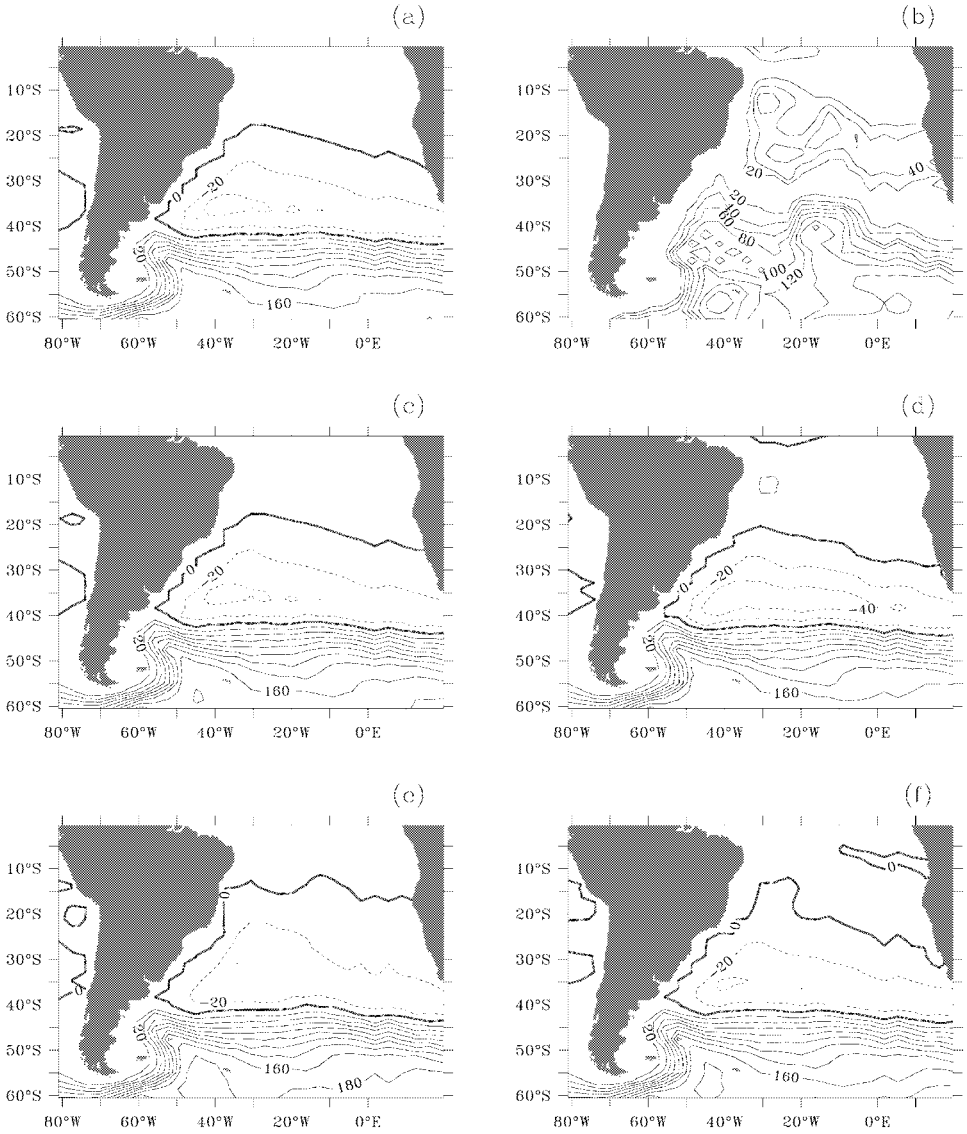

Figure 11. (a) PSI annual climatology for the pre-industrial period. (b) The associated variance (contour interval is 20 Sv^2 units). PSI seasonal climatology for the pre-industrial period : (c) summer; (d) autumn; (e) winter and (f) spring. Contour intervals is 20 Sv.

values appear in autumn to south of 45° S (Figure 14c), where the difference in transport reaches 25 Sv near 55° S–0° E, coincident with negative SST differences (Figure 6c). In the Subtropical Gyre the highest differences occur in spring (Figure 14e), when the transport increase in the center-southern part of the Subtropical Gyre is about 5 Sv.

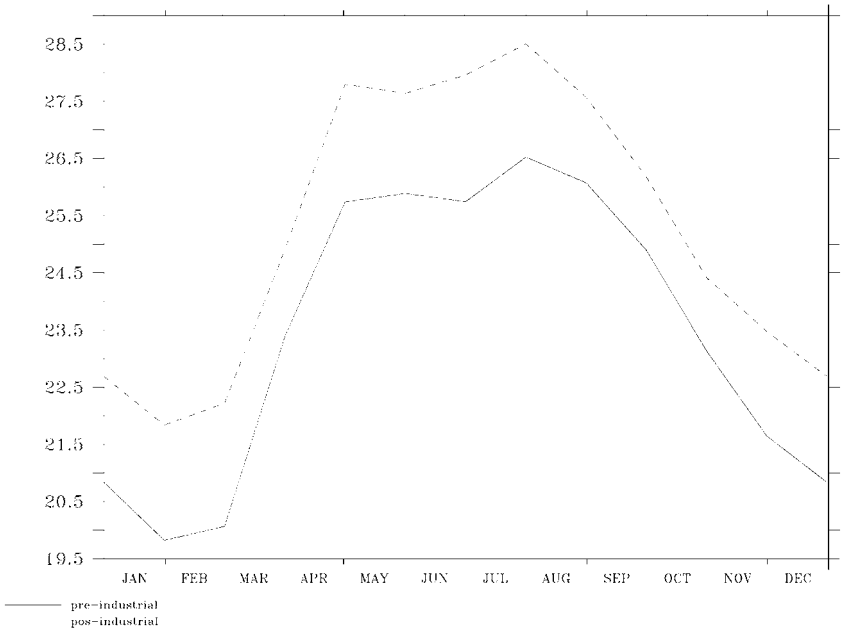

Figure 12. Annual cycle of PSI averaged for the whole South Atlantic domain in Sv. Black curve represents the pre-industrial simulation results while the dashed curve represents the present day results.

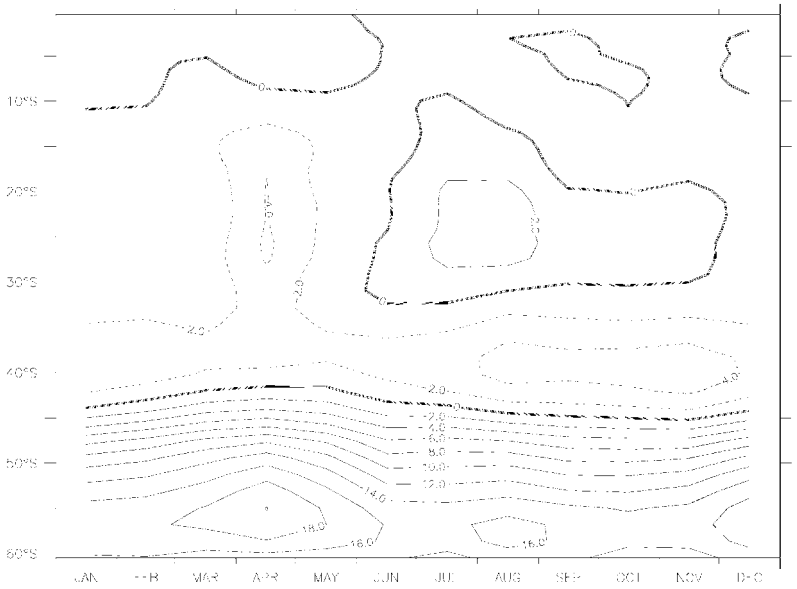

Figure 13. Difference between zonal mean PSI from the two simulations (present day–pre-industrial). Contour intervals is 2 Sv.

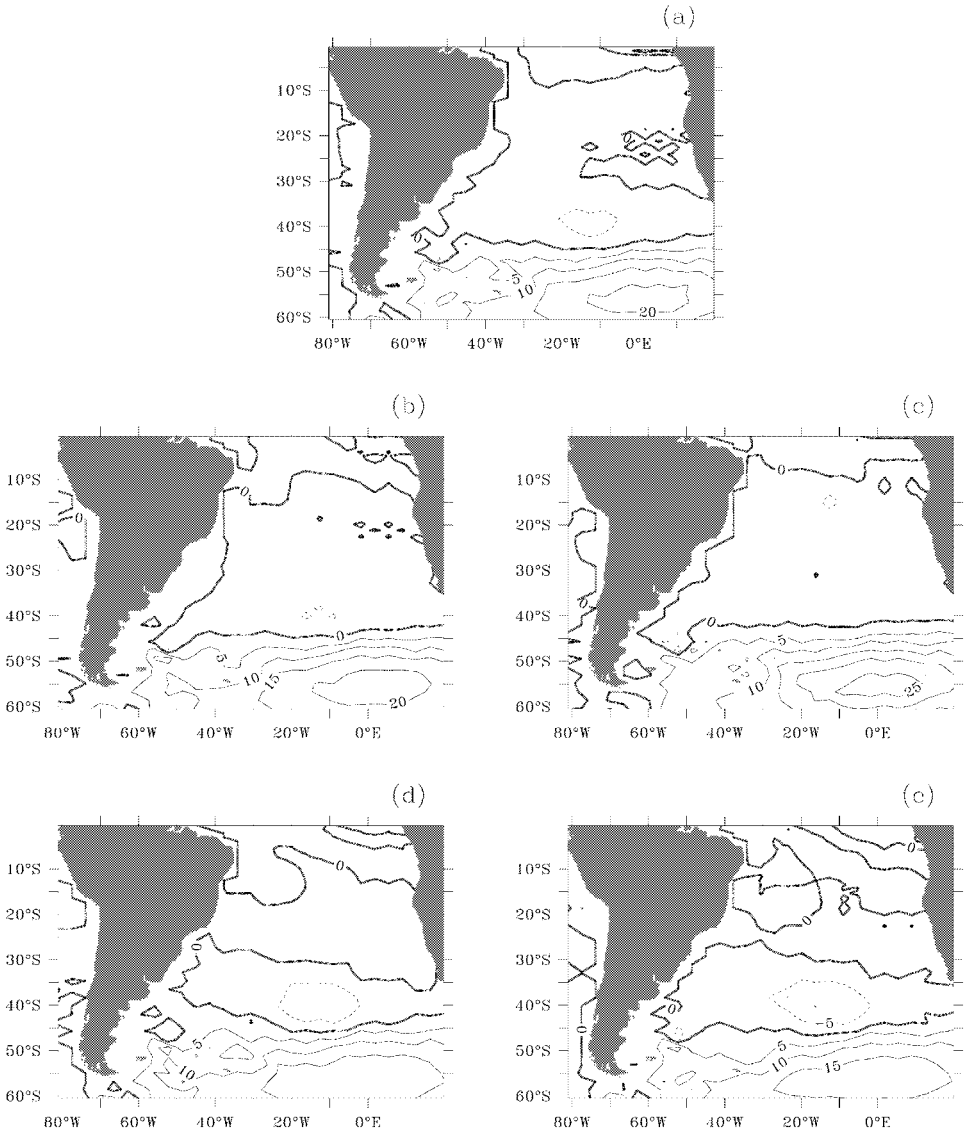

Figure 14. (a) PSI difference between the two simulations (present day–pre-industrial) for the annual climatology. Contour intervals is 5 Sv. PSI difference between the two simulations (present day–pre-industrial) for the seasonal climatology: (b) summer; (c) autumn; (d) winter and (e) spring.

3.4. CHANGES IN PRECIPITATION

Rainfall, both over land and ocean surface, is one of the most important climatic factors (together with temperature) for the nations that border the South Atlantic Ocean. This is because a major part of the economy of the region is dependent on rain-fed agriculture. Furthermore, extreme rainfall anomalies result into droughts

and floods, which are often associated with food, energy, water shortages, loss of life and property and many other socio-economic disruptions.

The Amazon Basin supports one of the three quasi-stationary centers of intense near-equatorial convection and is the largest and most intense land-based convective center. During the Southern Hemisphere summer when convection is best developed, the Amazon Basin is one of the wettest regions on earth (Liebman et al., 1998). Therefore, changes associated to climate change in this region are presented.

Figure 15a shows the annual climatology for precipitation (PPT) for the pre-industrial experiment. Higher values of PPT can be noticed over the tropical oceanic region and Amazon basin, as well as the associated variance (Figure 15b). Near the Andes PPT is also high basically due to its orographic nature, where moisture is transported by trade winds from the ITCZ. The Amazon region presents a mean PPT of approximately 2300 mm per year (Fish et al., 1996), consistent with the model output (about 2000 mm/year).

Seasonally, PPT is maximum in autumn, over tropical ocean at 20° W, 8° S, when it presents values as high as 45 mm/h (Figure 15d), due to the southward displacement of ITCZ. According to Hastenrath and Heller (1997), the ITCZ is farther displaced into the southern hemisphere in April. This meridional displacement of the ITCZ along the year is one of the most important agents that determine PPT in the northern part of Brazil.

Over the South American continent, the Amazon region exhibits considerable PPT during spring to autumn (Figures 15c,d,f), which can be associated with the Bolivian High (BH). In winter, the BH disappears and the maximum PPT shifts to north. Central Amazon is dominated by the descendent branch of the Hadley Cell, which combined with the BH disappearance, leads to climatological minimum values of PPT (less than 0.05 mm/h) during winter, as seen in Figure 15e. In spring (Figure 15f) PPT is higher over Amazon at the same area where SLP reaches its minimum values, as shown in Figure 7f. Following Fisch et al. (1996) maximum PPT is observed in Amazon basin between November and March, coherent with Figure 15. The South Atlantic Convergence Zone (SACZ) is underestimated in the model. The SACZ is a complicated region, where PPT rates are determined by the advection of moisture off the continent, wind convergence near the coast, and transient circulation.

Annual cycle of PPT over the whole domain (Figure 16) shows maximum values from February to April and minimum between July and November, for both experiments. Present days level simulation reveals less PPT from January to June months, especially in March when it is 0.014 mm/h lower than the pre-industrial experiment.

Looking at Figure 17 we can better examine the differences between zonal mean PPT from pre-industrial to post-industrial simulation. The main response of PPT due to the increase of greenhouse gases occurs at tropical latitudes. PPT is slightly intensified from September to November (0.01 mm/h) between 5° S to 20° S. How-

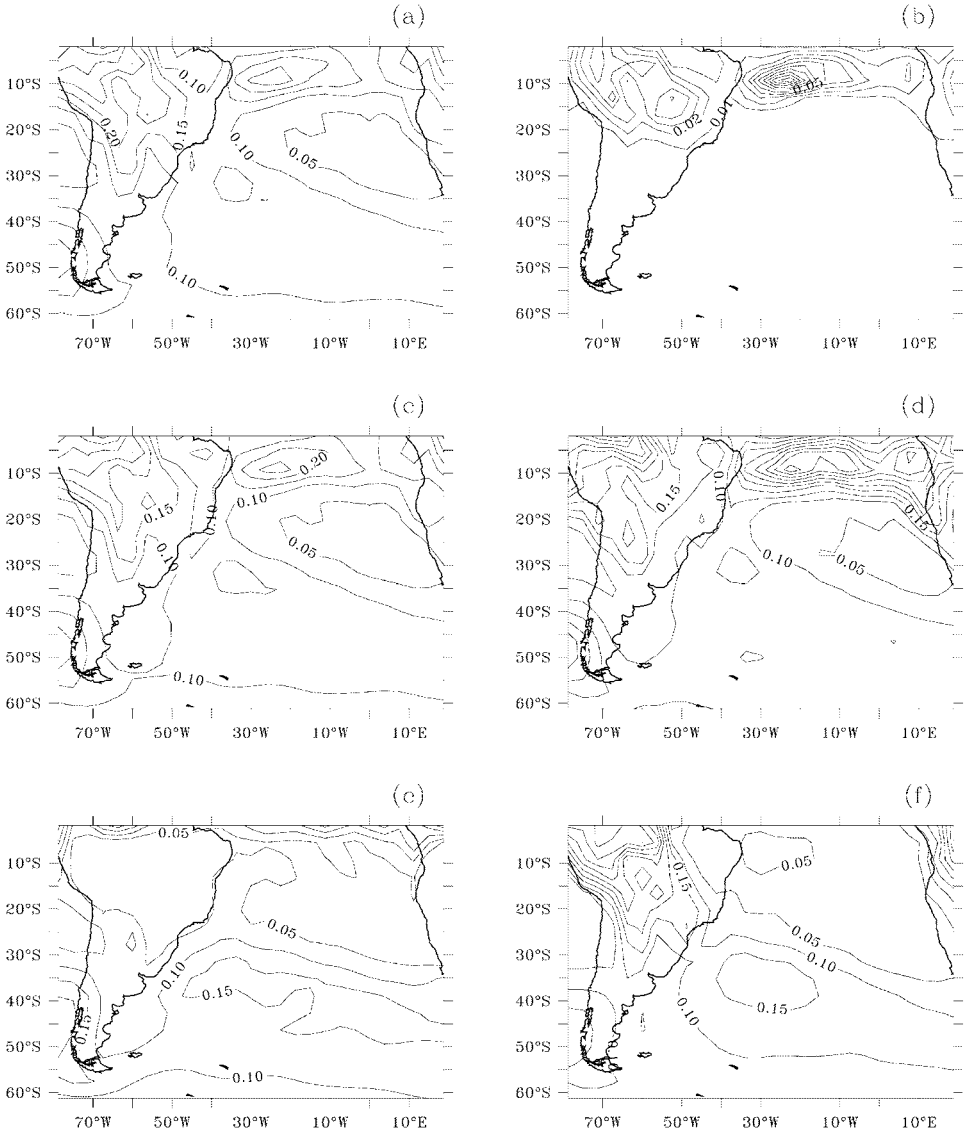

Figure 15. (a) PPT annual climatology for the pre-industrial period. (b) The associated variance (contour interval is 0.02 mm/h). PSI seasonal climatology for the pre-industrial period: (c) summer; (d) autumn; (e) winter and (f) spring. Contour intervals is 0.05 mm/h.

ever, the major feature is a PPT decrease at approximately the same latitudes, from January to May. The negative differences reach 0.07 mm/h in March. At the same period Figures 5 and 9 reveal a cooling of sea surface and the intensification of subtropical high, respectively. Studies have shown that tropical SST has some influence northeast Brazil rainfall by modulation of ITCZ position (Hastenrath

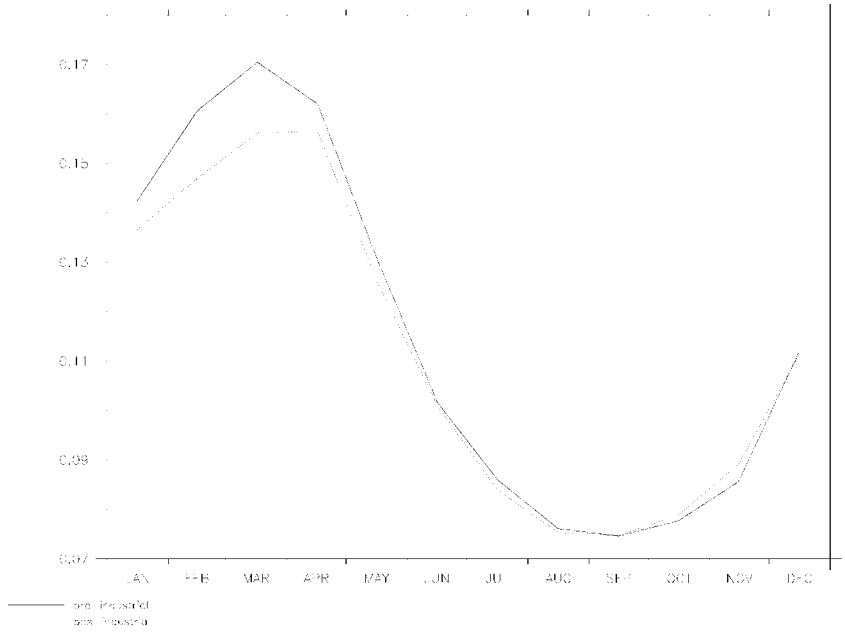

Figure 16. Annual cycle of PPT averaged for the whole domain in mm/h. Black curve represents the pre-industrial simulation results while the dashed curve represents the present day results.

and Heller, 1977; Moura and Shukla, 1981). Nobre and Shukla (1996) also found impacts of Atlantic tropical SST on rainfall in the central Amazon region.

Figure 18 presents the PPT differences between two simulations. In the annual mean, PPT (Figure 18b) intensifies over the South American continent, mainly at the Amazon, and over the western tropical ocean, where differences reach 0.03 mm/h around 5° S, 30° W. Over the South Atlantic, PPT decreases to north of 30° S approximately. In summer (Figure 18b) PPT is completely changed: almost the whole South American continent suffers an increase in precipitation, suggesting the intensification of ITCZ and SACZ. In counterpart, most of the South Atlantic reveals a decrease in PPT. Figure 18c shows the weakening of PPT during autumn, most concentrated between 5° S and 30° S, including the continental region. During this season, at similar latitudinal band, the sea surface is cooled (Figure 6c) and SLP is intensified (Figure 10c). Associated with these changes, trade winds are strengthened from pre-industrial to post-industrial experiment (not shown). A strengthening of PPT north of 5° S is also evident (Figure 18e). During winter (Figure 18d) the changes on PPT are lower and in the next season (Figure 18e) PPT increases basically over the continent, located at Amazon region.

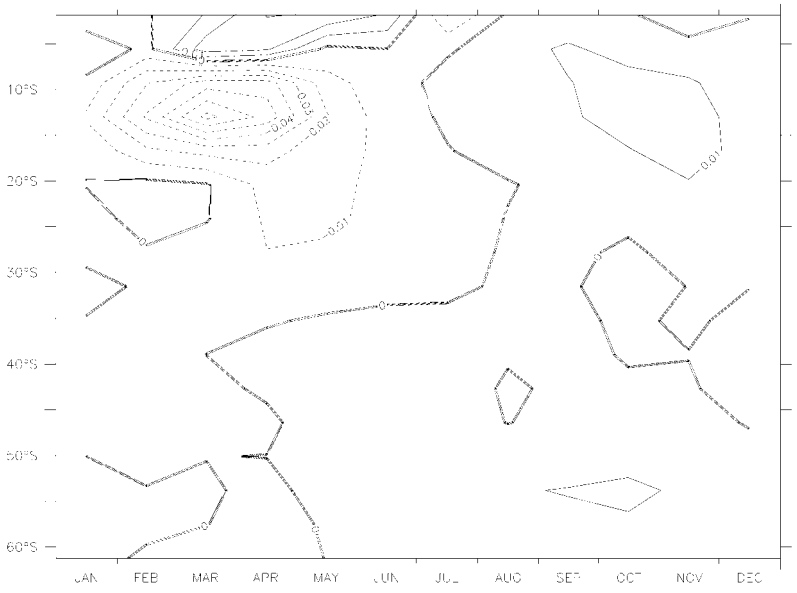

Figure 17. Difference between zonal mean PPT from the two simulations (present day–pre-industrial). Contour intervals is 0.02 mm/h.

4. Discussion

In an attempt to determine the impacts on the South Atlantic Ocean due to global warming, we have analyzed two numerical experiments from NCAR CCSM, based on changes in the greenhouse gas concentration from pre-industrial to present-day levels.

It has been already established with respect to the global mean average, that an increase of atmospheric greenhouse gas concentrations leads to an average increase of the temperature of the surface-troposphere system. The response of the climate system to greenhouse gas forcing is complex and involves many processes and feedbacks that interact non-linearly (IPCC report of working group I, 2001). Generally, the response does not scale with the amplitude of the forcing. This means that small perturbations can induce large changes in the climate system.

One point that should be noted is the different solar constant used in each experiment. The solar constant of 1365 Wm^{-2} was based on solar variability reconstructions and it is appropriate for the 19th century, i.e., pre-industrial conditions. The post-industrial run, nevertheless, uses the present-day value of the solar constant (1367 Wm^{-2}). The actual change in radiative forcing can be estimated by taking the difference in the solar constants (2 Wm^{-2}) divided by 4 (area of disk of intercepted solar radiation divided by surface area of earth) times (1 minus the planetary albedo), which means 0.35 Wm^{-2}. This result is much smaller than the radiative forcing due to changes in the greenhouse gases (about 1.5–2 Wm^{-2}). Since 1850, the climate forcing of 2.4 Wm^{-2} induced by greenhouse gas exceeds

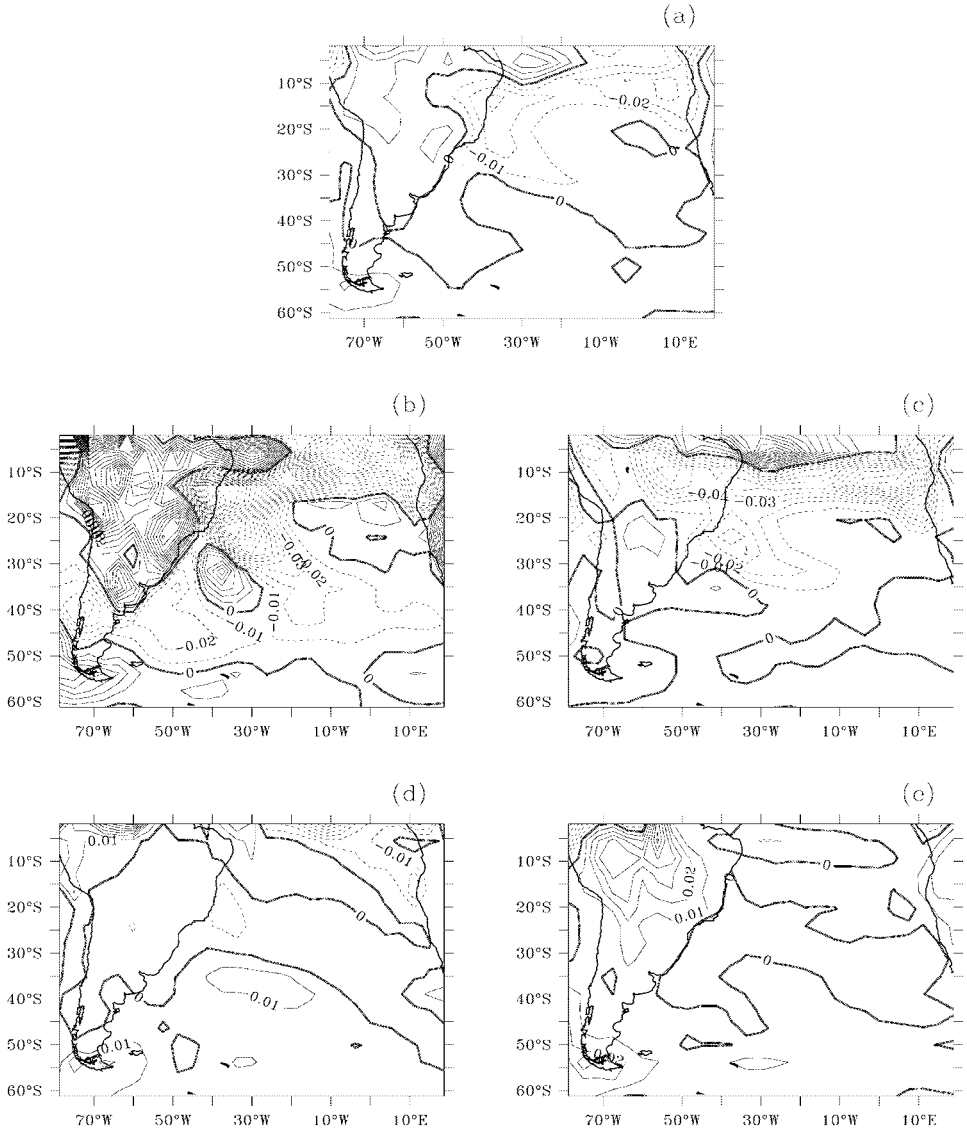

Figure 18. (a) PPT difference between the two simulations (present day–pre-industrial) for the annual climatology. Contour intervals is 0.02 mm/h. PSI difference between the two simulations (present day–pre-industrial) for the seasonal climatology: (b) summer; (c) autumn; (d) winter and (e) spring.

that by solar forcing, thought to be in the range of 0.2–0.8 Wm^{-2} (Frohlich, 1998; Soon et al., 1996; Solanki and Fligge, 1998).

Comparison of the simulation results between present-day levels of greenhouse/trace gases and pre-industrial period levels shows that the largest difference (for the most part positive) are located at high latitudes (south of at least 45° S). These results are consistent with previous findings where no warming had been

Table I
Summary of the annual average difference between experiments for SST, SLP, PSI and PPT divided by regions

Spatial domain	SST (°C)	SLP (mb)	PSI (Sv)	PPT (mm/year)
South Atlantic	0.64	0.31	3.35	–8.00
0–25° S	0.41	0.22	0.49	–21.53
25–45° S	0.67	0.40	1.87	–9.31
45–60° S	0.92	0.39	11.25	25.25

observed north of about 42° S (discussed in Houghton et al, 1995). In fact, observational studies performed in Chile (approximately 50° S) indicate that mean surface temperatures showed no increasing trend before 1900 and that during the period 1900–1990, the temperature in the Southern Hemisphere increased by a total of 0.4 °C, at a fairly constant rate (Rosenbluth et al., 1997).

The Table I summarizes the differences between periods for the annual average for the whole South Atlantic for the region averaged between the equator-25° S, between 25–45° S and for the region between 45–60° S. It can be verified that in the annual average, the whole region experiences intensification which is weaker between the equator and 40° S and gets stronger south of it. Considering that the climatology was calculated for monthly averages of a 150 years run (i.e., large number of samples) it is believed that the differences found between runs are very robust and do not reflect random climate fluctuations.

The biggest changes observed for the averaged SST not only occurred between 40°S and 55°S but they happened during spring. It should be mentioned that a considerable cooling was observed during autumn in the center-north portion of the basin (Figure 6c) between the two experiments with differences of the order of 0.8 °C. SST also decreases in present-day experiments at the ACC region during autumn, reducing the strong gradient of warming observed in other seasons. SLP revealed the greatest differences during the summer months, mainly at the westerly wind region while during winter a reduction could be noted. However, as noted in Table I, it was the barotropic transport that presented greatest changes, maximum in autumn (Figure 14c) consistent with the intensification of the SLP and the decrease in SST at the ACC region. Changes in SLP are related to alteration in wind stress, which in turn affects the oceanic transport. The strengthening of PSI at high latitudes during the autumn season results in more cold water flowing to north, cooling the sea surface. The intensification of PSI at the southern part of the subtropical gyre during winter and spring (Figures 14d,e) provides a strengthening of transport to the south, which, combined with the northward transport of cold

waters at high latitudes, contributes to the strong SST gradient at the polar front region.

PPT showed significant changes in its seasonal cycle, mainly at tropical latitudes during summer and autumn. The distribution of PPT over the South American continent, at Amazon region, is intensified in summer and spring and weakened during autumn. During summer, the SACZ is also intensified. Although Table I shows bigger PPT differences at high latitudes, the tropics suffered more with the increase of greenhouse gases. PPT at high latitudes slightly increase during almost all the year resulting in considerable rise in accumulated PPT. On the other hand, average PPT differences at tropical region had great variations along the year.

Changes in transport are a special concern since there is the possibility of reduction of the Atlantic thermohaline circulation caused by warming and freshening of high latitude surface water associated with global warming as shown by Manabe and Stouffer (1994) and Stocker and Schmittner (1997). Both the high latitude warming and an enhanced poleward transport of moisture in the atmosphere contribute to the reduction of water density in the bottom water formation regions.

5. Critique

It should be pointed out that although this paper deals mainly with the equilibrium changes in the climatology of the South Atlantic ocean-atmosphere system within a coupled GCM study, the real climate system is undergoing transient change. The equilibrium scenarios reproduced here, where the difference between two climates was used as an estimate of the sensitivity of the South Atlantic climate system, may not produce the same time-evolving patterns of climatic changes as do transients (i.e., time dependent climate response). Nonetheless, even if the mechanisms behind these changes may remain unclear, it is believed that this study may shed some light to the areas in the South Atlantic region (mainly the higher latitudes) most sensitive to a global warming scenario originating from increased greenhouse gases.

Even though this study focused on the climate mean state, it should be noted that there is substantial variability at interannual and lower frequencies in both coupled simulations examined. The next step (well underway) is to identify the modes of variability of each experiment and try to understand why they change.

Acknowledgements

This work was supported in part by grants FAPESP-00/02958-7, FAPESP-02/01211-0, CNPq 300223/93-5, CNPq 300561/91-1, CNPq 300040/94-6. CNPq/MMA 550363/02-5. I. W. thanks SGER/NSF and NCAR for travel funds. NCAR is sponsored by the National Science Foundation. We also thank the FERRET support group.

References

Bonan, G.: 1998, 'The Land Surface Climatology of the NCAR Land Surface Model Coupled to the NCAR Community Climate Model', *J. Climate* **11**, 1307–1326.

Boville, B. and Gent, P. R.: 1998, 'The NCAR Climate System Model, Version One', *J. Climate* **11**, 1115–1130.

Bradley, R., Diaz, H., Eischeid, J., Jones, P., Kelly, P., and Goodess, C.: 1987, 'Precipitation Fluctuations over Northern Hemisphere Land Areas since the Mid-Nineteenth Century', *Science* **237**, 171–175.

Cane, M., Clement, A., Kaplan, A., Kushnir, Y., Pozdnyakov, D., Seager, R., Zebiak, S., and Murtuguddenatuer, R.: 1997, 'Twentieth-century Sea Surface Temperature Trends', *Science* **275** (5302), 957–960.

Crowley, T.: 2000, 'Causes of Climate Change over the Past 1000 Years', *Science* **289** (5477), 270–277.

Da Silva, A., Young, A., and Levitus, S.: 1994, 'Atlas of Surface Marine Data 1994, Volume 1: Algorithms and Procedures', in *NOAA Atlas NESDIS 6*, U.S. Department of Commerce, Washington, D.C.

Danabasoglu, G.: 1998, 'On the Wind-Driven Circulation of the Uncoupled and Coupled NCAR Climate System Ocean Model', *J. Climate* **11**, 1442–1454.

Delworth, T. L. and Knutson, T. R.: 2000, 'Simulation of Early 20th Century Global Warming', *Science* **287**, 2246–2250.

Fisch, G., Marengo, J. A., and Nobre, C. A.: 1996, *Clima da Amazônia*, Climanálise Especial-Edição comemorativa de 10 anos. CPTEC/INPE, Brazil.

Flato, G. M. and Hibler, W. D.: 1992, 'Modeling Ice Pack as a Cavitating Fluid', *J. Phys. Oceanogr.* **22**, 626–651.

Frohlich, C. and L. J.: 1998, 'The Sun's Total Irradiance: Cycles, Trends and Related Climate Change Uncertainties since 1976', *Geophys. Res. Lett.* **25**, 4377–4380.

Garzoli, S.: 1999, 'The Relevance of the South Atlantic for Climate Studies', *Clivar Exchanges* **13**, 35–37.

Gent, P., Bryan, F., Danabasoglu, G., Doney, S., Holland, W., Large, W., and McWilliams, J. C.: 1998, 'The NCAR Climate System Model Global Ocean Component', *J. Climate* **11**, 1287–1306.

Gille, S. T.: 2002, 'Warming of the Southern Ocean since the 1950s', *Science* **295**, 1275–1277.

Hack, J. J., Kiehl, J. T., and Hurrell, J.: 1998, 'The Hydrologic and Thermodynamic Characteristics of the NCAR CCM3', *J. Climate* **11**, 1179–1206.

Hansen, J., S. M., L. A., Ruedy, G. R., and M. E.: 1998, 'Climate Forcings in the Industrial Era', in *Proceedings of the National Academy of Sciences*, Vol. 12, pp. 753–758, 9.

Hastenrath, S.: 1991, *Climate Dynamics of the Tropics*, Kluwer Academic Publishers, New York, p. 488.

Hastenrath, S. and Heller, L.: 1977, 'Dynamics of Climatic Hazards in Northeast Brazil', *Q. J. R. Meteorol. Soc.* **103**, 77–92.

Hellerman, S. and Rosenstein, M.: 1983, 'Normal Monthly Wind Stress over the World Ocean with Error Estimates', *J. Phys. Oceanogr.* **13**, 1093–1104.

Houghton, J., Callander, B., and Varney, S.: 1992, *Climate Change 1992: The Supplementary Report to the IPCC Scientific Assessment*, Cambridge University Press, New York.

Houghton, J. T. e.a.: 1995, *Climate Change 1995 – The Science of Climate Change*, Cambridge University Press, Cambridge.

Kiehl, J. T., Jack, J. J., Bonan, G., Boville, B. A., Williamson, D., and Rasch, P.: 1998, 'The National Center for Atmospheric Research Community Climate Model: CCM3', *J. Climate* **11**, 1131–1149.

Levitus, S., Antonov, J., Boyer, T., and Stephens, C.: 2000, 'Warming of the World Ocean', *Science* **287** (5461), 2225–2229.

Liebman, B., Marengo, J., Glick, J., Kousky, V., Wainer, I., and Massambani, O.: 1998, 'Comparison of Rainfall, Outgoing Longwave Radiation, and Divergence over the Amazon Basin', *J. Climate* **11** (11), 2898–2909.

Manabe, S. and Stouffer, R.: 1994, 'Multiple-century Response of a Coupled Ocean-atmosphere Model to an Increase of Atmospheric Carbon-dioxide', *J. Climate* **7** (1), 5–23.

Manabe, S., Wetherald, R., and Stouffer, R.: 1981, 'Summer Dryness Due to an Increase of Atmospheric CO_2 Concentration', *Clim. Change* **3**, 347–385.

Matear, R. J. and Hirst, A.: 1999, 'Climate Change Feedback on the Future Oceanic CO_2 Uptake', *Tellus* **51** (3), 722–733.

McCabe, G. J., Clark, M., and Serreze, M.: 2001, 'Trends in Northern Hemisphere Surface Cyclone Frequency and Intensity', *J. Climate* **14** (12), 2763–2768.

Mitchell, J. F. B.: 1989, 'The Greenhouse Effect and Climate Change', *Rev. Geophys.* **27** (1), 115–139.

Petit, J. R., Jouzel, J., Raynaud, D., Barkov, N. I., Barnola, J., Basile, M. B. I., Chapellaz, J., Davis, M., Delaygue, G., Delmotte, M., Kotlyakov, V. M., Legrand, M., Lipenkov, V. Y., Lorius, C., Pepin, L., Ritz, C., Saltzman, E., and Stievenard, M.: 1999, 'Climate and Atmospheric History of the Past 420,000 Years from the Vostok Ice Core, Antarctica', *Nature* **399**, 429–436.

Rayner, N. A., Parker, D. E., Horton, E. B., Folland, C. K., Alexander, L., Rowell, D. P., Kent, E. C., and Kaplan, A.: 2003, 'Global Analyses of SST, Sea Ice and Night Marine Air Temperature since the Late Nineteenth Century', *J. Geophys. Res.* **108** (D14), 4407, doi:10.1029/2002JD002670.

Reid, J.: 1989, 'On the Total Geostrophic Circulation of the South Atlantic Ocean: Flow Patterns, Tracers and Transports', *PO* **23**, 149–244.

Reynolds, R. W. and Smith, T. M.: 1994, 'A High Resolution Global Sea Surface Temperature Climatology', *J. Climate* **7**, 929–948.

Rosenbluth, B., Fuenzalida, H., and Aceituno, P.: 1997, 'Recent Temperature Variations in Southern South America', *Int. J. Clim.* **17**, 67–85.

SACC: 1996, *South Atlantic Climate Change*, Technical Report, NOAA/AOML/PhOD.

Schimel, D., Alves, D., Enting, I., Heimann, M., Joos, F., Raynaud, D., Wigley, T., Prather, M., Derwent, R., Ehhalt, D., Fraser, S., Sauhueza, E., Zhou, X., Jonas, P., Charlson, R., Rodhe, S., Sadasivan, H., Shine, K., Fouquart, Y., Ramaswamy, V., Solomon, S., Srinivasan, J., Albritton, D., Derwent, R., Isaksen, I., Lal, M., and W. D.: 1996, *Radiative Forcing of Climate Change*, Cambridge University Press, Cambridge, U.K.

Solanki, S. K. and Fligge, M.: 1998, 'Solar Irradiance since 1874 Revisited', *Geophys. Res. Lett.* **25**, 341–344.

Soon, W. H., P., E. S., and Baliunas, S. L.: 1996, 'Inference of Solar Irradiance Variability from Terrestrial Temperature Changes, 1880–1993: An Astrophysical Application of the Sun-Climate Connection', *Astrophys. J.* **472**, 891–902.

Stocker, T. and Schmittner, A.: 1997, 'Rate of Global Warming Determines the Stability of the Ocean-Atmosphere System', *Nature* **388**, 862–865.

Stott, P. A., T., S. F. B., Jones, G. S., Allen, M. R., Ingram, W. J., and Mitchell, J. F. B.: 2001, 'Attribution of Twentieth Century Temperature Change to Natural and Anthropogenic Causes', *Clim. Dyn.* **17**, 1–21.

Stouffer, R. J., Manabe, S., and Bryan, K.: 1989, 'Interhemispheric Asymmetry in Climate Response to a Graudal Increase of Atmospheric CO_2', *Nature* **342**, 660–662.

Stramma, L. and Peterson, R.: 1989, 'Geostrophic Transport in the Benguela Current Region', *J. Phys. Oceanogr.* **19**, 1440–1448.

Wainer, I., Gent, P. R., and Goni, G.: 2000, 'The Annual Cycle of the Brazil-Malvinas Confluence Region in the NCAR Climate System Model', *J. Geophys. Res.* **105**, 26176–26178.

Weatherly, J. W., Briegleb, B. P., Large, W. G., and Maslanik, J. A.: 1998, 'Sea Ice and Polar Climate in the NCAR CSM', *J. Climate* **11**, 1472–1486.

Wigley, T. M. L. and Raper, S.: 1987, 'Thermal Expansion of Sea Water Associated with Global Warming', *Nature* **247**, 127–131.

(Received 28 May 2002; in revised form 3 December 2003)